JOURNAL OF GEOPHYSICAL RESEARCH, VOL. 113, A09209, doi:10.1029/2008JA013257, 2008

Origin of Saturn's aurora: Simultaneous observations by Cassini and the Hubble Space Telescope

E. J. Bunce,[1] C. S. Arridge,[2] J. T. Clarke,[3] A. J. Coates,[2] S. W. H. Cowley,[1] M. K. Dougherty,[4] J.-C. Gérard,[5] D. Grodent,[5] K. C. Hansen,[6] J. D. Nichols,[3] D. J. Southwood,[4,7] and D. L. Talboys[1]

Received 4 April 2008; revised 29 May 2008; accepted 25 June 2008; published 5 September 2008.

[1] Outer planet auroras have been imaged for more than a decade, yet understanding their physical origin requires simultaneous remote and in situ observations. The first such measurements at Saturn were obtained in January 2007, when the Hubble Space Telescope imaged the ultraviolet aurora, while the Cassini spacecraft crossed field lines connected to the auroral oval in the high-latitude magnetosphere near noon. The Cassini data indicate that the noon aurora lies in the boundary between open- and closed-field lines, where a layer of upward-directed field-aligned current flows whose density requires downward acceleration of magnetospheric electrons sufficient to produce the aurora. These observations indicate that the quasi-continuous main oval is produced by the magnetosphere-solar wind interaction through the shear in rotational flow across the open-closed-field line boundary.

Citation: Bunce, E. J., et al. (2008), Origin of Saturn's aurora: Simultaneous observations by Cassini and the Hubble Space Telescope, *J. Geophys. Res.*, *113*, A09209, doi:10.1029/2008JA013257.

1. Introduction

[2] During an era of high-resolution remote imaging of planetary auroras using the Hubble Space Telescope (HST), whilst spacecraft sample in situ outer planet magnetospheres, the origin of the aurora is a topic of interest and debate. It is now generally understood that the main auroral emissions at Jupiter originate in field-aligned currents (FACs) flowing in the magnetosphere-ionosphere coupling current system associated with the breakdown of iogenic plasma corotation in the middle magnetosphere [*Cowley and Bunce*, 2001; *Hill*, 2001; *Southwood and Kivelson*, 2001], although the precise details of their modulation is not yet resolved. The auroral emissions in the Jovian ionosphere are highly complex, however, and are produced by a variety of different mechanisms, from the moon-related emissions at lowest latitudes, to the highly-variable polar emissions which may be solar wind driven at highest latitudes [see *Clarke et al.*, 2004]. However, consideration of the related magnetosphere-ionosphere coupling currents in Saturn's middle magnetosphere does not account for the auroras that are observed, an assertion concluded both from the magnitude and mapped location of the field-aligned current densities. This led to the suggestion that they are therefore most likely the result of the solar wind interaction with Saturn's magnetosphere [*Cowley and Bunce*, 2003; *Cowley et al.*, 2004a], more like the situation at Earth. Quantitative modeling by *Cowley et al.* [2004b] (hereafter referred to as the 'CBO' model) specifically suggests that Saturn's auroras are associated with a ring of upward-directed FAC spanning the boundary between open and closed magnetic field lines. The current is generated by the difference in plasma angular velocity between open field lines at high-latitudes that strongly sub-corotate with respect to the planet, and closed outer magnetosphere field lines at lower latitudes that near-rigidly corotate. In brief, this work predicts that (1) upward FACs occur at the open-closed-field line boundary typically located at $\sim$15° colatitude, (2) that the upward FAC density, estimated to be $\sim$150 nA m^{-2}, requires downward field-aligned acceleration of magnetospheric electrons through a $\sim$10 kV potential such that the precipitating electron energy flux is sufficient to produce UV intensities of a few tens of kR (where 1R = 10^{10} photons m^{-2} s^{-1} into 4π sr) in the upper atmosphere, and (3) the currents will be larger and the aurora brighter at dawn than dusk when the solar wind-driven Dungey cycle is active. An alternative suggestion by *Sittler et al.* [2006] places the aurora on closed-field lines mapping to the outer ring current region of the middle-outer magnetosphere.

[3] HST observations indicate a UV auroral intensity at Saturn which is typically several tens of kR [*Gérard et al.*, 2004], and an oval which generally resides between 14°–16° colatitude in the southern hemisphere [*Cowley et al.*,

[1]Department of Physics and Astronomy, University of Leicester, Leicester, UK.
[2]Mullard Space Science Laboratory, University College London, Dorking, UK.
[3]Center for Space Physics, Boston University, Boston, Massachusetts, USA.
[4]Blackett Laboratory, Imperial College, London, UK.
[5]Laboratoire de Physique Atmosphérique et Planétaire, Université de Liège, Liège, Belgium.
[6]Department of Atmospheric, Oceanic, and Space Sciences, University of Michigan, Ann Arbor, Michigan, USA.
[7]European Space Agency, HQ, Paris, France.

0148-0227/08/2008JA013257$09.00

2004a; *Badman et al.*, 2006], in basic agreement with the CBO model. In addition, the highly variable nature of the auroral emissions in response to upstream solar wind disturbances observed during an HST campaign in January 2004 [*Clarke et al.*, 2005] agrees well with the overall theoretical framework presented by *Cowley et al.* [2005]. However, such evidence is merely circumstantial, and in situ measurements of the auroral current system and its location are required to provide definitive evidence concerning its physical origin. Here, for the first time, we present near-simultaneous observations of the southern auroras at Saturn using HST UV images and concurrent Cassini measurements of auroral FACs in the polar magnetosphere.

2. Observations

2.1. Remote UV Observations

[4] As part of a large coordinated HST-Cassini campaign during January–February 2007, daily observations of Saturn's southern hemisphere aurora were made at UV wavelengths using the Advanced Camera for Surveys (ACS) on the HST. In Figure 1 we show two images from the campaign obtained on consecutive visits, which have been projected onto a polar latitude-longitude grid as though viewed "through" the planet looking from the North. Image A shows the sum of 5 individual exposures obtained during 06:40–06:50 UT on 16 January 2007 corresponding to a "Saturn time" of 05:31–05:41 UT (HST time minus the 69 min light travel time from HST to Saturn), while image B similarly shows the sum of 5 exposures taken during 04:30–04:39 UT on 17 January corresponding to a Saturn time of 03:21–03:30 UT. General effects associated with the projection and summation of HST images is discussed in a general sense by *Grodent et al.* [2005]. The white dotted circles indicate lines of constant colatitude, and are plotted at 5° intervals. Noon is at the bottom of each image, dawn to the left and dusk to the right. The image is truncated on the nightside because of increasing uncertainty in the polar projections toward the limb of the planet. Within the region shown, the auroral distribution in these images is somewhat spread due both to the finite resolution of the instrument, and by projection effects. The instrument resolution contributes ~1° spread near the noon oval, while projection effects, particularly due to the finite height of the auroral curtain, may contribute a further ~1.5°. The combined colatitude spread due to these effects is thus likely to be ~2° in the vicinity of the noon oval. These images were obtained during Rev 37 of the Cassini spacecraft about Saturn. The white track in Figure 1 indicates the magnetically-mapped ionospheric footprint of the Cassini spacecraft for the interval 10–23 January 2007, with the white dots marking six-hourly intervals. Magnetic mapping in the CBO model used the internal field model of *Davis and Smith* [1990] combined with the ring current model of *Connerney et al.* [1983] model, while here we use a combination of the new "Cassini" internal field model for Saturn [*Dougherty et al.*, 2005], and a typical ring current model derived from recent analysis of Cassini data [*Bunce et al.*, 2007, 2008]. The ring current model employed here is specifically for a typical sub-solar magnetopause position of ~21 R_S, though other choices make only marginal differences. For example, if the sub-solar magnetopause value increases to 26 R_S (the maximum value in the *Bunce et al.* [2007] model, implying the most extended magnetosphere) the mapped spacecraft position moves equatorward by ~0.5°. Therefore over the full sub-solar magnetopause range of the *Bunce et al.* [2007] ring current model (i.e., between 16–26 R_S) we would expect colatitudinal changes of only ±0.5° to those shown in the figure. The mapped position of Cassini at the Saturn time of each image is indicated by the red spot, while the green line shows the interval of upward FAC signatures at Cassini to be discussed later.

[5] In these images the UV auroral oval (shown in blue tones according to the color scale on the right-hand side) is seen as an approximately circumpolar band displaying a variety of familiar characteristics. Near to noon the oval lies between ~10°–15° colatitude, and has a peak brightness of ~30 kR (the mean brightness across the oval at ~12 LT is ~15 kR). The oval is also asymmetric between dawn and dusk, the aurora forming a brighter and more discrete feature at dawn than at dusk. A contraction of the emission is also seen between images A and B, suggesting a possible solar wind-related effect similar to but less extreme than that observed during January 2004 [*Clarke et al.*, 2005; *Badman et al.*, 2005]. To examine this possibility in Figure 2 we show the dynamic pressure of the solar wind propagated from the Earth to Saturn using the 1-D MHD model of *Zieger and Hansen* [2008], for the interval discussed in this paper. We see evidence that the magnetosphere underwent a corotating interaction region shock-compression at the start 15 January, where we see a sharp increase in the solar wind dynamic pressure from 0.006–0.05 nPa, marked by the dotted vertical line. The timing uncertainty for the propagated pressure values in this model is ±15 hours, such that the shock-compression arrival time may be reasonably assumed to be between ~12:00 UT on 14 January and ~12:00 UT on the 15 January. The dashed vertical lines in Figure 2 marked A and B then indicate the times of the two HST images. The Saturn Kilometric Radiation (SKR) observations are also a good indicator of the activity in the solar wind [*Kurth et al.*, 2005], and inspection of this data during the interval of interest reveals a compression-related signature at the beginning of 15 January, and also subsequent active bursts of emission spanning the next couple of days (W.S. Kurth, personal communication, 2008). These subsequent bursts of SKR are timed well with subsequent smaller enhancements in the solar wind dynamic pressure seen in Figure 2. The contraction of the auroral oval between images A and B may therefore relate generally to the magnetospheric response to the arrival of the shock-compression at the boundary of the magnetosphere near the beginning of day 15, and the subsequent activity which follows [e.g., *Cowley et al.*, 2005].

[6] Figure 1 shows that the spacecraft footprint was located poleward of the oval in image A at ~8° colatitude in the pre-noon sector, while being equatorward of the oval at ~15° colatitude in image B. The differences of ±0.5° in the spacecraft mapped footprint that would result from using different ring current model parameters (as discussed above) could not place the spacecraft footprint in image A equatorward of the oval, or shift it poleward of the oval in image B. Thus it is apparent that, as indicated by the white

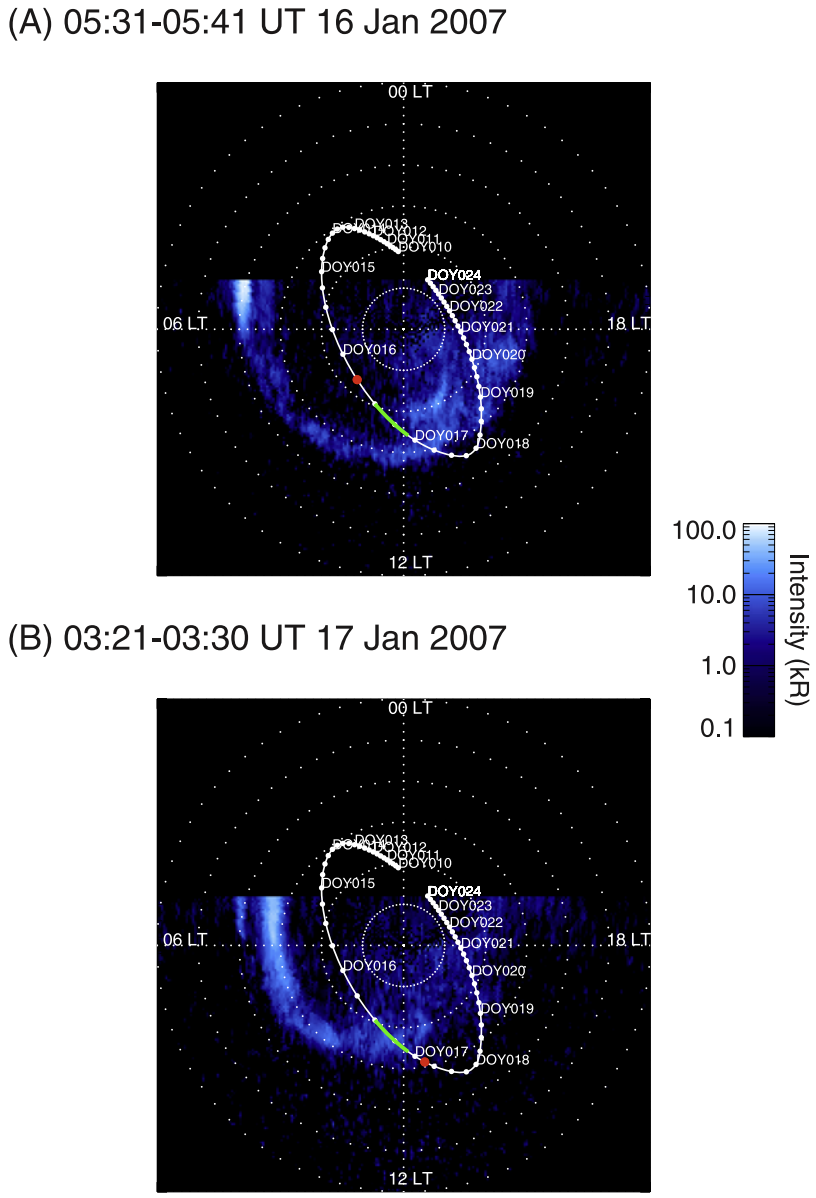

Figure 1. Plot showing two consecutive ACS HST images of Saturn's UV aurora. Image A is a sum of 5 exposures taken between 05:31 and 05:41 UT 16 January 2007, while image B is similarly a sum of 5 exposures taken between 03:21 and 03:30 UT 17 January 2007. The polar grid shows the southern hemisphere as if viewed through the planet from the north. As such, noon is toward the bottom of each image, dawn to the left, and dusk to the right. The white dotted circles indicate lines of constant colatitude and are plotted at 5° intervals. The right-hand side color bar indicates the UV brightness in kR on a logarithmic scale. The white track indicates the magnetically mapped footprint (see text for discussion of magnetic field model employed) of the Cassini spacecraft during days 10–24 of 2007 for comparison. In each case, the red dots indicate the position of the spacecraft at the central time of the summed exposures in image A and image B. The extended green line indicates the region of upward FAC signatures seen in the Cassini magnetic field data discussed later in the text.

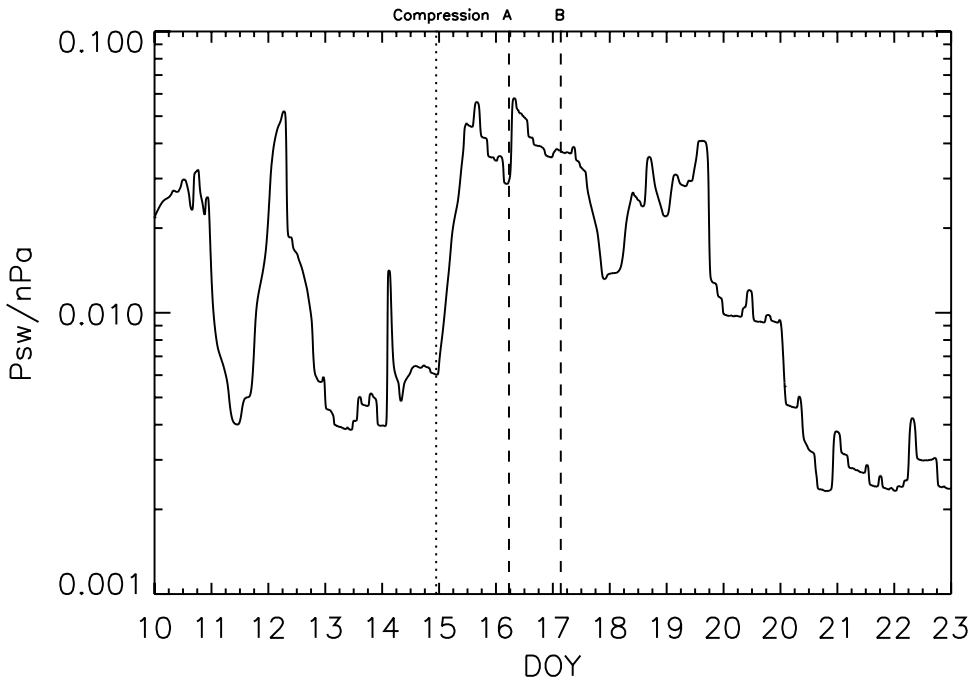

Figure 2. Plot showing the dynamic pressure of the solar wind in units of nPA, propagated from Earth to Saturn according to the 1-D MHD model of *Zieger and Hansen* [2008] as a function of UT. The vertical dotted line indicates the start of a compression region within the solar wind, while the dashed lines show the times of images A and B for comparison.

track, the footprint of the spacecraft crossed the auroral oval between the two images from a poleward location in image A to an equatorward location in image B, such that Cassini must have been located on auroral flux tubes during a portion of the intervening interval. We therefore now investigate the field and plasma data obtained by Cassini during this interval.

2.2. In Situ Cassini Observations

[7] We begin our discussion of the concurrent Cassini data by presenting in Figure 3 the trajectory of the spacecraft during Rev 37, shown in the coordinate system where the z-axis is aligned with the planet's rotation axis, and the x–z plane contains the Sun. We show three views of the spacecraft trajectory given by the solid lines, labeled at the start of even days and marked with dots at six hourly intervals throughout. The figure shows projections onto (1) the equatorial x–y plane, (2) the noon–midnight x–z plane, and (3) the dawn–dusk y–z plane. The dashed curves in Figures 3a and 3b show extreme magnetopause positions, for solar wind dynamic pressures of $P_{sw} = 0.01$ and 0.1 nPa, obtained from the model of *Arridge et al.* [2006] derived from Cassini data. We see from Figure 3a that during this orbit, Cassini moved from post-midnight at the start of day 10, through the dawn sector on day 15, and reached the noon meridian at the end of day 16. The spacecraft then moved through dusk and back toward midnight between day 18 and 23. In Figures 3b and 3c we note that the spacecraft crossed the planet's equator from north to south on day 13 in the post-midnight sector, and back again at the end of day 17 in the post-noon sector. With reference to Figure 1, we note that on days 16 and 17 the spacecraft traversed auroral latitudes in the southern ionosphere, very near to noon. The times at which auroral images A and B were obtained are again shown by the red dots in each, while the green line also shows the interval of upward FAC signatures at Cassini shortly to be discussed.

[8] In Figure 4 we show the in situ magnetic field and plasma electron data from Cassini during Rev 37 over an interval spanning 10 Earth days, from day 10 to 20 2007. The data in the top show measurements of thermal electrons in the energy range ~0.6 eV–26 keV, made by the Cassini electron spectrometer (CAPS-ELS). Beneath this, the magnetic field data are presented in spherical polar components referenced to the planet's spin/magnetic axes, B_r, B_θ, and B_φ respectively, together with the magnitude of the field $|B|$ shown in the bottom, all in units of nT. The dotted lines in each indicate the "Cassini" internal planetary field model [*Dougherty et al.*, 2005]. Since the model field is axisymmetric and has no azimuthal component, no dashed line is shown in the B_φ panel. The universal time, radial distance, colatitude of the spacecraft measured from the northern axis, and local time are indicated at the bottom. The two vertical dashed lines marked (A) and (B) indicate the center Saturn times of the images in Figure 1, while three vertical solid lines mark the two equatorial crossings during this orbit (N to S and S to N), and the point of closest approach (CA) to Saturn on day 16.

[9] At the start of the interval on day 10 the spacecraft was located at high latitudes in the northern hemisphere, where an absence of electrons above a few tens of eV is observed in the ELS spectrogram in the first panel (the lower energy electrons are spacecraft photoelectrons). The magnetic field observed at this time was quiet and strongly radial, indicative of a low beta region corresponding to the northern tail lobe (beta is the ratio of the plasma pressure to

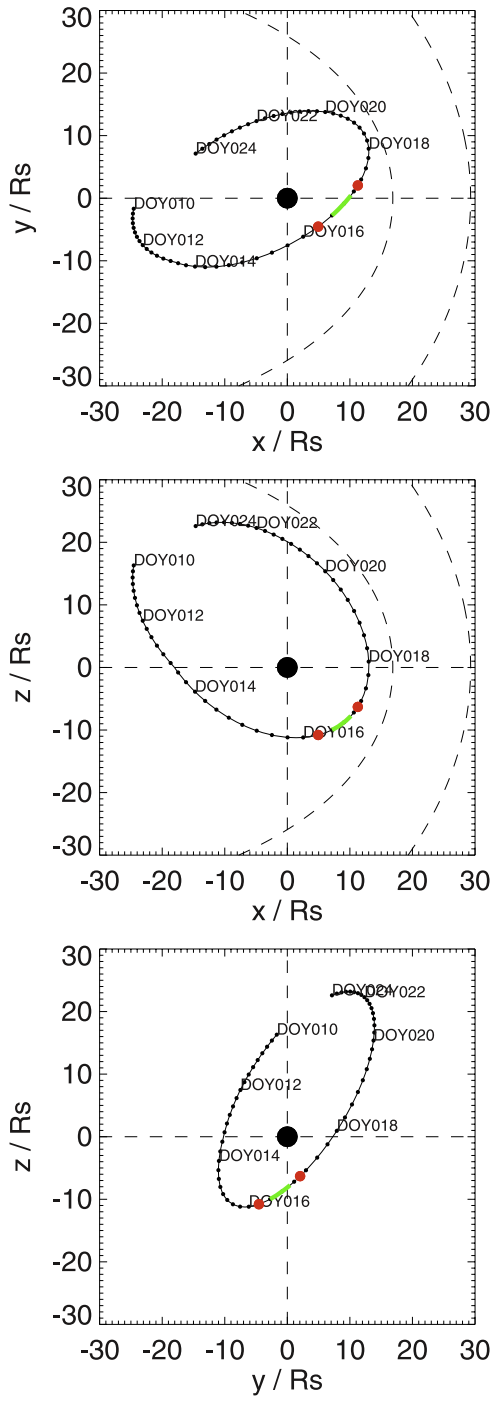

Figure 3. Cassini trajectory for the Rev 37 interval (i.e., days 10–24 2007) in a coordinate system where the z direction points along Saturn's spin/magnetic axis, and the x–z plane contains the Sun. Figures 3a–3c show the x–y plane (equatorial), the x–z plane (noon–midnight), and the x–y plane (dawn–dusk) respectively. As in Figure 1, the red dots indicate the position of the spacecraft at the times of images A and B, and the green track indicates the region of upward FAC signatures in the Cassini field data.

the field pressure). At ~06:00 UT on day 13, the spacecraft crossed through the equatorial plane in the post-midnight sector. During this crossing the magnetic field became temporarily disturbed, indicating the presence of hot plasma associated with the tail current sheet, as seen in the electron data (in the 100–1000 eV range) in the first panel. Interestingly, both data sets indicate a sequence of entries into the tail current sheet on day 11 followed by multiple crossings of its center, on days 12 and 13, associated with the strong oscillations in the field components seen throughout the interval. The B_r and B_φ components of the field finally switched sign as the spacecraft moved into the southern hemisphere on day 13. Following entry into the southern hemisphere, the spacecraft moved into a region of quiet, near-radial field following some further periodic encounters with the plasma sheet on days 13 and 14. The quiet radial nature of the field after this time, until ~10 UT on day 16, indicates that during this interval the spacecraft was located on open field lines mapping between Saturn's southern polar cap and the solar wind. This conclusion is strongly supported by the evidence provided by the observed particle populations. It can be seen in Figure 4 that the quiet field region was entirely devoid of warm plasma electrons, similar to conditions observed in the northern lobe in day 10. Such regions devoid of warm plasma were also observed on a number of adjacent Cassini orbits when the spacecraft reached similar high magnetic latitudes, such that the overall data shown in Figure 4 follow a commonly-observed pattern. However, it is also commonly observed in low-latitude Cassini data that warm ~keV quasi-isotropic electrons are observed whenever the spacecraft crosses the magnetopause onto closed outer magnetospheric field lines, similar to the warm populations observed later in the interval shown in Figure 4 as will be discussed further below. However, a quasi-isotropic warm electron population would be observed at essentially similar intensities at all points along a closed-field line, thus leading to the conclusion that the central region in Figure 4 devoid of warm electrons is not so connected, but is rather connected to the southern lobe. This conclusion is also supported by the energetic ion and electron fluxes measured concurrently by the Cassini MIMI/LEMMS instrument [not shown; N. Krupp, personal communication], which were at the background level throughout most of this "void" region, ~2 orders of magnitude less than values typical of the outer magnetosphere. Further comments on this conclusion will be provided below.

[10] A remarkable feature of the magnetic field data in the region we have identified as mapping to the southern lobe is the presence of a positive azimuthal component, which persists and grows throughout the morning sector and toward noon. The sense of this component indicates that these field lines are being twisted in the sense of planetary rotation in the southern ionosphere, indicative of strong subcorotation of the plasma on these high-latitude field lines. However, shortly after the time of image A a large-amplitude perturbation began in the magnetic field components. In particular, the azimuthal field switched back and forth over an interval of ~10 h following ~12:00 UT on day 16 between strong positive values of ~5–10 nT, and near-zero and slightly negative values that were continuous after ~22:00 UT. From Ampères law, this reduction in B_φ is indicative of a layer of net upward-directed FAC (away from the planet), to be quantified in section 3, which was thus traversed by the spacecraft as it crossed the auroral oval between the times of image A and image B. The reduction

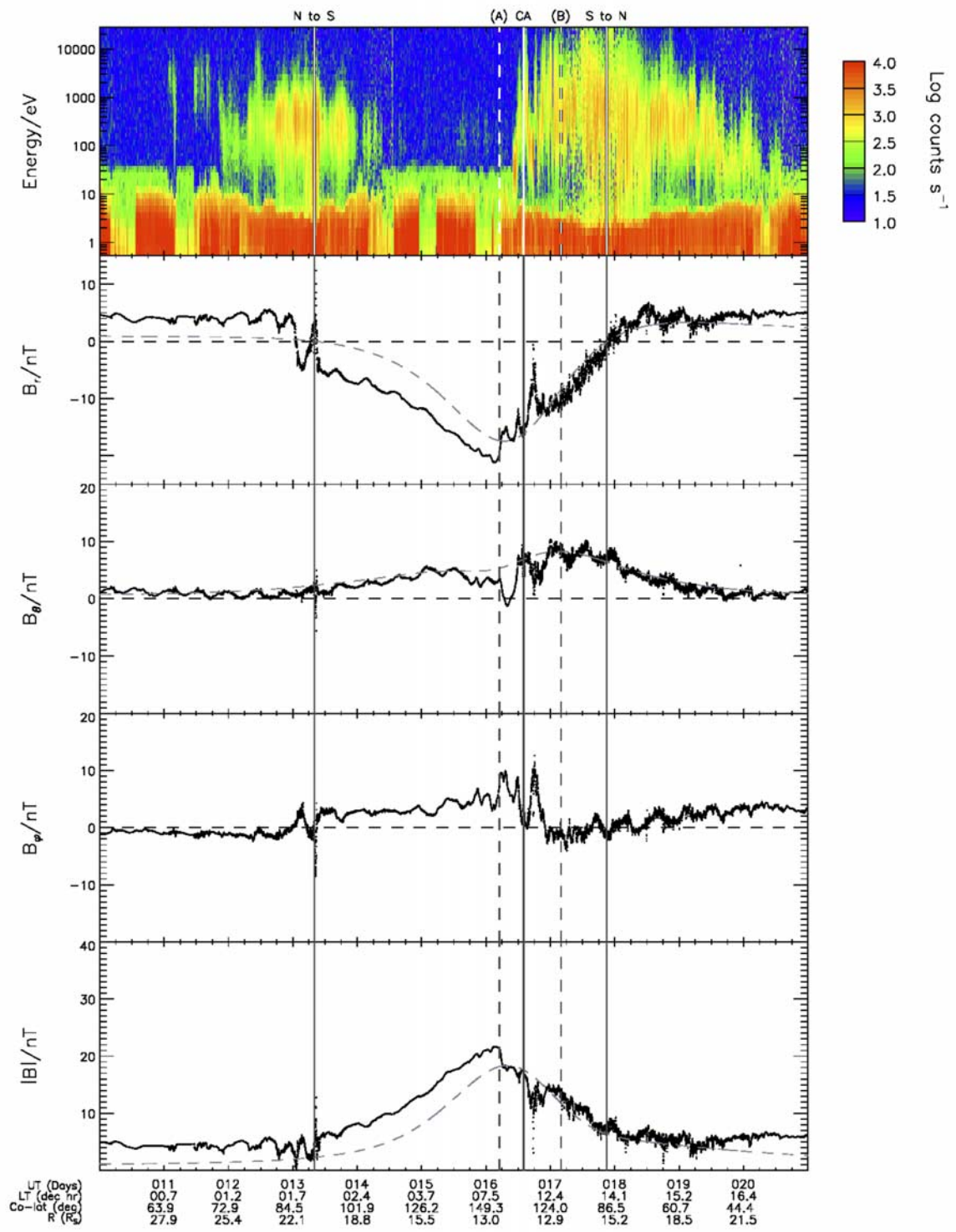

Figure 4. Overview plot of Cassini magnetic field and thermal electron data during days 10–20 of 2007. The first panel shows a CAPS-ELS spectrogram over the energy range 0.6 eV to 26 keV, with the logarithmic color scale on the right-hand side indicating the counts s^{-1} of electrons in that range. The following three panels indicate the magnetic field components in spherical coordinates, B_r, B_θ, and B_φ all in units of nT. The fourth panel shows the total field strength. The dotted line indicates the internal field model for Saturn [*Dougherty et al.*, 2005]. Trajectory information is shown at the bottom of the plot, specifically the time (days), spacecraft local time (hours), colatitude (degrees), and radial distance (R_S). The solid vertical line marked CA shows the time of closest approach of the spacecraft. The vertical solid lines with N to S and S to N marked at the top indicate the timings of the north to south and south to north equator crossings, respectively. Finally, the vertical dashed lines shows the timings of the HST images A and B.

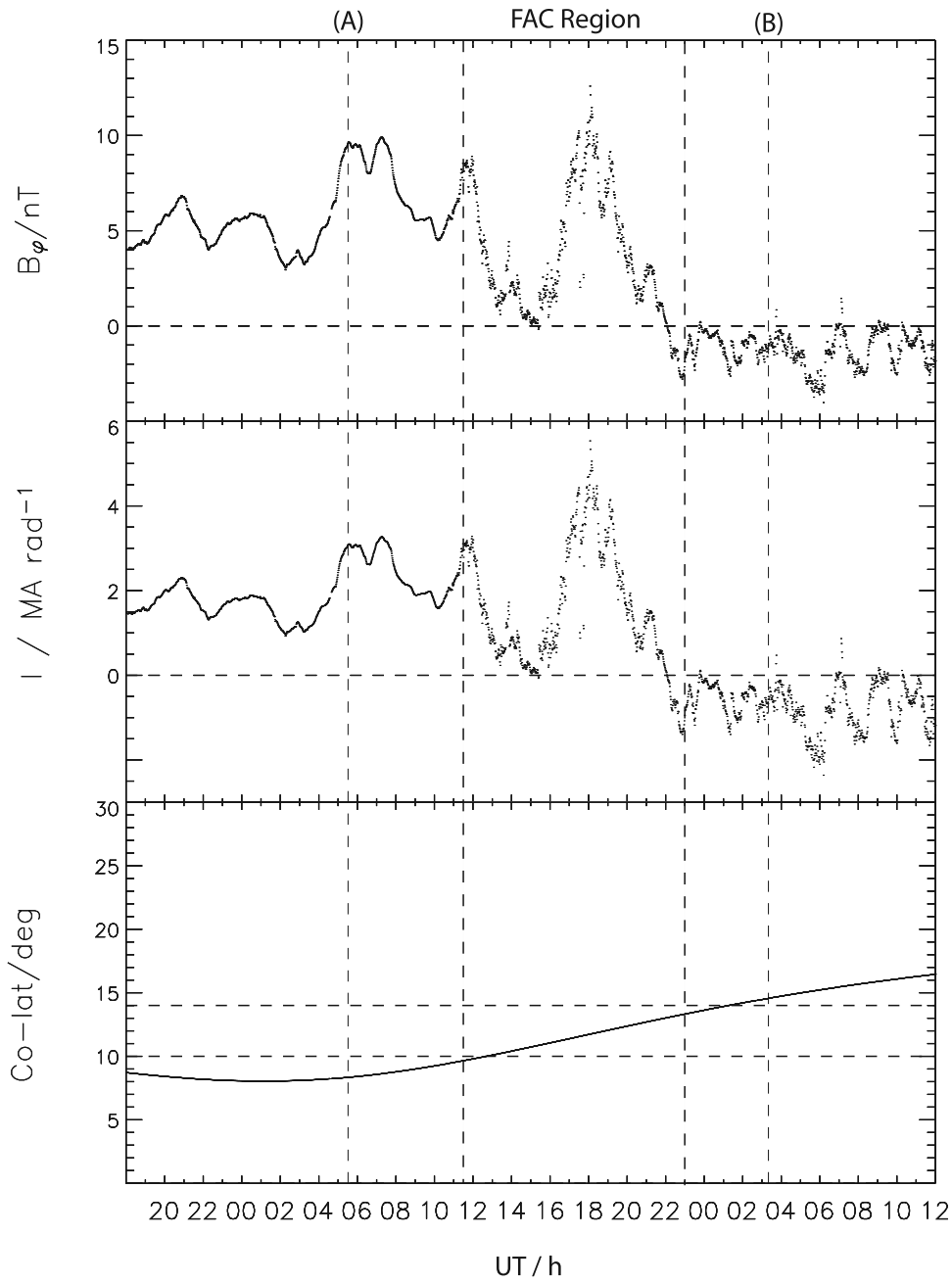

Figure 5. Stacked plot of the azimuthal field component B_φ (nT) from 18:00 UT on day 15 to 12:00 on day 17 2007, the implied equatorward directed ionospheric Pedersen current per radian of azimuth, I, at the ionospheric feet of the spacecraft field lines (MA rad^{-1}), and the mapped ionospheric colatitude of the spacecraft. The dashed horizontal lines in the bottom indicate the equatorward and poleward edges of the auroral oval in image B for comparison. The outer pair vertical dashed lines show the time of images A and image B. The region of upward FAC is also indicated by the inner pair of dashed lines at ~11:30 UT and at ~23:00 UT on day 16.

in azimuthal field may be interpreted as being due to an increase in plasma angular velocity to near-corotational (or even slightly super-corotational) values, which strongly reduced (or even slightly reversed) the ionospheric torque. It was in this regime that Cassini was located at the time of image B, when the ionospheric footprint of the spacecraft lay equatorward of the auroral oval (Figure 1). We may comment that this overall behavior of B_φ is also commonly observed on adjacent orbits with similar characteristics, such that it is clearly a spatial rather than a temporal phenomenon.

[11] The switch in B_φ between ~12:00–22:00 UT on day 16 is accompanied by a change from quiet (low-β) field to fluctuating field associated with the presence of hot plasma. The nature of the transition in plasma properties can be seen in the first panel, where we see that the electron fluxes are

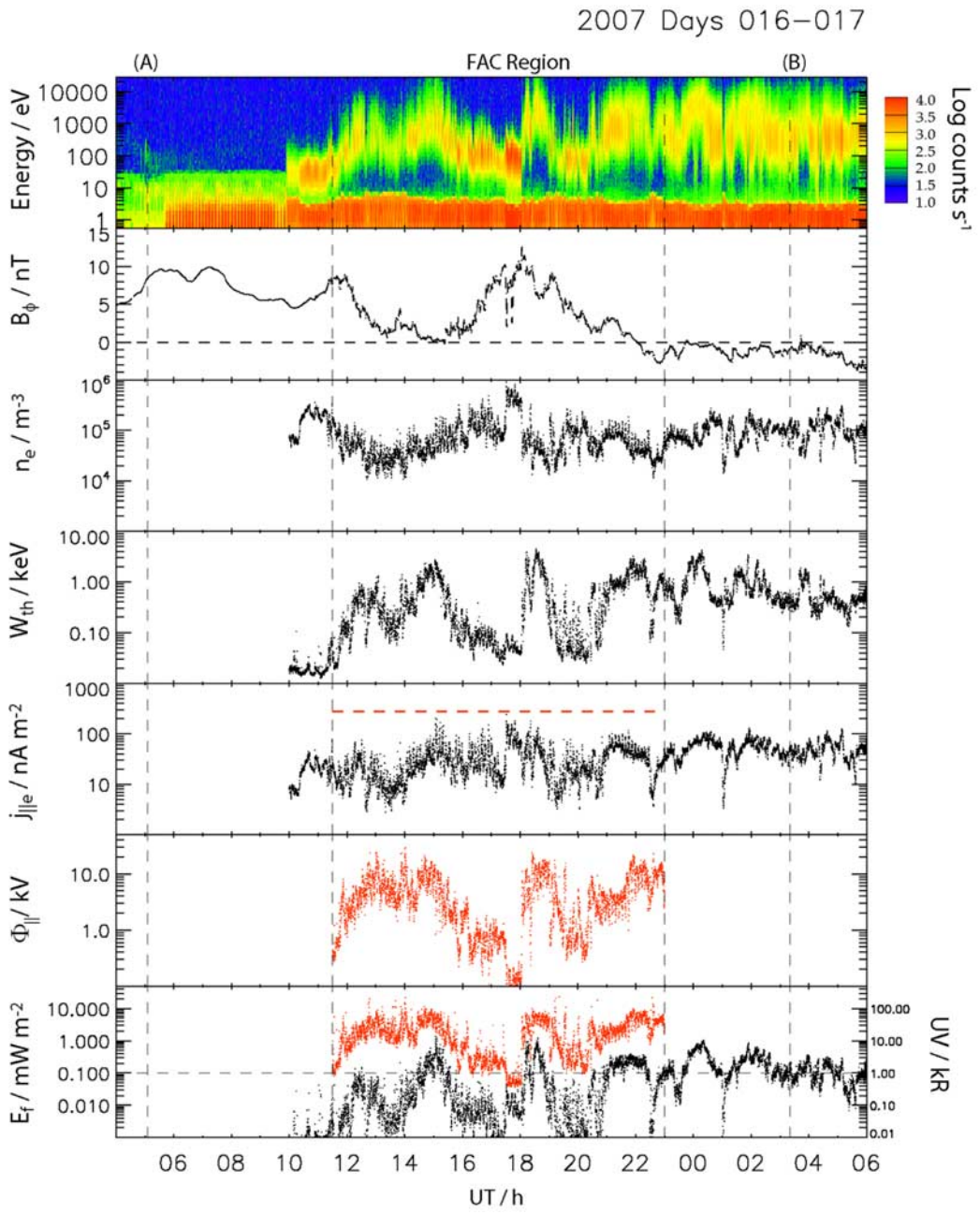

Figure 6. Stacked plot of electron parameters observed by Cassini within the B_φ transition region, together with derived auroral parameters, shown for the interval from 04:00 UT on day 16 to 06:00 UT on day 17 of 2007. The first panel shows a CAPS-ELS spectrogram in the same format as Figure 4, while the second panel shows the azimuthal field component B_φ in nT. The third and fourth panels show the electron density n_e (m^{-3}) and temperature W_{th} (keV) derived from the CAPS-ELS data. In the fifth panel, the black dots indicate the source electron current density for electrons moving in one direction along the field lines, $j_{\|e}$ (nA m^{-2}), also derived from the CAPS-ELS electron flux measurements, with the red dashed line at 275 nA m^{-2} indicating the calculated ionospheric field-aligned current density, $j_{\|i}$ (see section 3). The sixth panel shows the accelerating potential, $\Phi_\|$ (kV) required by the measured electron population to carry the ionospheric current density shown in the fourth panel, according to the kinetic theory of *Knight* [1973] (equation (3a)). Finally, in the seventh panel, the black dots indicate the electron energy flux for electrons moving in one direction along the field lines, E_f (mW m^{-2}), derived from the CAPS-ELS data, while the postaccelerated energy flux at the ionosphere is shown by the red dots (equation (3b)). On the right-hand side, the equivalent UV kR intensity scale is indicated, with the dashed horizontal line depicting the limiting sensitivity of the ACS instrument. As in Figure 5, the outer pair of dashed vertical lines indicates the times of image A and B, while the inner pair shows the FAC region seen in the magnetometer data.

ordered by the field behavior. In the transition region, we see that dense and cool (10–100 eV) plasma electrons typical of the magnetosheath are present where B_φ has significant positive values. At this time (~18:00 UT), a strong diamagnetic effect in the field is also seen. The magnetic field strength (in the fourth panel) is significantly reduced because of the pressure of the magnetosheath-like plasma, and the principal component in the field changes from radial to azimuthal. As B_φ reduces to small values this cool population is replaced by warm electrons (100–1000 eV), typical of the outer closed-field magnetosphere. Between these two distinct populations, there is a ~1 h interval of hot electrons with energies beyond 10 keV, between ~18 and 19 UT on day 16, which is bounded on either side by cool electrons (see expanded plot in Figure 6). The overall transformation of the electron population from the "void" region at high latitudes, to magnetosheath-like electrons, and then to outer magnetosphere characteristics at lower latitudes, that occurs during the B_φ transition from positive to near-zero values, again indicates that the spacecraft crossed the boundary between open and closed-field lines, specifically in the region of the dayside "cusp" near to noon. We suggest that the hot electrons within the transition region are likely to be accelerated magnetosheath electrons on open field lines, a suggestion which is supported by analysis of the distribution functions of the electrons during this interval. Further discussion of these populations will form part of a more detailed analysis in preparation by C.S. Arridge and coworkers. The field then remained disturbed as the spacecraft moved clear of the boundary and entered the dayside magnetosphere proper.

[12] Overall therefore, we suggest these data show that Saturn's auroral oval lies in the boundary between open and closed-field lines, where a layer of net upward-directed FAC flows due to a shear in plasma angular velocity from subcorotational to near-corotational values across the boundary, in agreement with previous theoretical modelling [*Cowley et al.*, 2004a, 2004b].

3. Interpretation of Magnetic Field Signatures

[13] We now estimate the strength of the FAC density in the cusp ionosphere implied by the changes in the azimuthal field, and then in section 4 discuss the requirements for magnetospheric electron acceleration. Application of Ampère's law to a circular path of radius ρ centered on the spin and magnetic axis of the planet, assuming approximate axisymmetry at least locally, shows that the equatorward-directed height-integrated Pedersen current per radian of azimuth, I, flowing in the ionosphere at the feet of the field lines that pass through the path, is given by

$$I = \frac{\rho B_\varphi}{\mu_o}, \tag{1}$$

where B_φ is the azimuthal field component observed on the path, and μ_o is the permeability of free space. By current continuity, I is then equal to the net FAC per radian of azimuth flowing into the ionosphere between the pole and the spacecraft footprint. If I therefore increases by ΔI as we move toward the equator, then that amount of FAC per radian of azimuth must enter the ionosphere between these points. Similarly, if I decreases by ΔI on moving toward the equator, then that amount of FAC per radian of azimuth must have left the ionosphere. Therefore I increasing toward the equator implies a downward FAC, while I decreasing toward the equator indicates an upward FAC.

[14] To estimate the FAC density just above the ionosphere, we divide the change in the Pedersen current, ΔI, by the area of the region in which the current change occurs in the ionosphere. Assuming that the region corresponds to a narrow layer of width $\Delta\theta_I$ radians in colatitude, located at θ_I, the area per radian of azimuth is $R_I^2\,(\theta_I)\sin\theta_I\,\Delta\theta_I$ where $R_I\,(\theta_I)$ is the radius of the ionosphere at θ_I (where we assume an oblate spheroid as in the work of *Cowley and Bunce* [2003]). The field-aligned current density just above the ionosphere is then

$$j_{\|I} = \frac{\Delta I}{R_I^2(\theta_I)\sin\theta_I\Delta\theta_I}. \tag{2}$$

For example, a change in I of ~5 MA rad^{-1} over 1° of colatitude at ~15° yields an ionospheric current density of ~480 nA m^{-2}.

[15] The first panel in Figure 5 shows B_φ measured between 18:00 UT on day 15 and 12:00 UT on day 17, spanning the cusp interval of Figure 4, while the second shows the ionospheric current I computed on this basis from equation (1). The region of intermediate values indicative of strong FAC is bounded by the inner pair of vertical dashed lines, located between the times of HST images A and B marked by the outer pair vertical dashed lines. The third panel of Figure 5 shows the spacecraft colatitude mapped magnetically to the southern ionosphere as in Figure 1, together with the approximate width of the oval in image B. It can be seen that the inferred FAC region is closely colocated with the spacecraft traversal of the auroral oval, as also indicated by the green lines along the spacecraft track in Figures 1 and 3. The implication of the I values in the second panel of Figure 5 is that a net upward current of ~5 MA rad^{-1} flowed along the field lines within the oval region.

[16] As mentioned above, however, large-amplitude variations in B_φ occur in the boundary region, suggesting either multiple spatial structures or a single boundary structure that oscillates across the spacecraft. On the spatial interpretation, two large-scale upward FAC regions occur where I decreases with time, observed between ~11:30–15:00 UT and ~18:00–23:00 UT on day 16, separated by a large-scale region of downward FAC where I increase with time. This total FAC layer corresponds to a region in the ionosphere of width ~3.8°. The changes in I then show that the currents flowing in the two upward-FAC layers are $\Delta_I \sim 3$ and ~5.5 MA rad^{-1} respectively. Since these upward FACs map to the ionosphere in individual layers of width $\Delta\theta_I = 1.2°$ and 1.6°, respectively, the implied FAC densities just above the ionosphere are ~280 and ~320 nA m^{-2}. Overall, the total width of the FAC region corresponds well to the width of the aurora near to noon in image B. However, it is not clear that there are two distinct arcs present (associated with the two distinct upward FAC regions), although this may be a consequence of image resolution and projection procedures. On the temporal interpretation, a single layer of upward FAC carrying

$\sim$5 MA rad^{-1} oscillates across the spacecraft. In this picture, the spacecraft was in contact with the oscillating upward FAC layer throughout the region of intermediate B_φ values observed between $\sim$11:30 and 23:00 UT. Consideration of the peaks and troughs in the B_φ profile suggests that the oscillation amplitude of the layer was comparable with its width, in which case the FAC layer is roughly half the width of the overall boundary region observed by the spacecraft. On this basis we estimate a current layer of $\sim$1.9° width carrying a total current of $\sim$5 MA rad^{-1}. The associated ionospheric FAC density is then $\sim$270 nA m^{-2}. We note that this width is narrower than the oval seen in image B, such that on this interpretation the oval must have widened to that seen in the image in the intervening 4.5 h.

[17] Overall, however, either interpretation produces estimates of the ionospheric current density of $\sim$250–300 nA m^{-2}, which we note is a factor of $\sim$2 larger than that predicted by the CBO model. As we now show, such current densities are of sufficient magnitude to require acceleration of magnetospheric electrons into the ionosphere, resulting in auroral emissions of several tens of kR as observed.

4. Electron Acceleration and Auroral Brightness

[18] The peak value of the FAC density on a given field line occurs just above the ionosphere. When this value exceeds that provided by the total field-aligned flux of magnetospheric electrons, which is constant on a given field line for a near-isotropic population, the electrons must be accelerated downward into the ionosphere by a field-aligned voltage. Here we show that such acceleration is indeed required above Saturn's oval in the present case, and estimate the accelerating voltage and energy flux of the precipitating electrons. These calculations employ the kinetic theory of *Knight* [1973], who shows that acceleration of magnetospheric electrons along field lines into the ionosphere is required if the ionospheric FAC density, $j_{\|I}$, exceeds that provided by the total flux of magnetospheric electrons moving along the field toward the ionosphere, $j_{\|e}$, this being constant on each field line (and in all directions in space on that field line) if the source electron population is isotropic, as we assume. In this case, Knight's theory shows that the minimum field-aligned accelerating voltage $\Phi_\|$ and the associated precipitating accelerated electron energy flux E_{fI} are given by

$$e\Phi_\| = W_e\left(j_{\|I}/j_{\|e}\right) - 1\right) \tag{3a}$$

and

$$E_{fI} = \left(E_{fe}/2\right)\left(\left(j_{\|I}/j_{\|e}\right)^2 + 1\right), \tag{3b}$$

where W_e and E_{fe} are the thermal energy and energy flux of the unaccelerated source electrons, respectively.

[19] Results are shown in Figure 6 for a 26 h interval spanning the cusp FAC region. For ease of cross-comparison with Figures 4 and 5, the top two panels show an electron spectrogram and B_φ, respectively, while the vertical dashed lines delimit the region of intermediate B_φ values constituting the cusp FAC region marked in Figure 5. The current is upward-directed throughout this region on the assumption that the FAC layer is oscillatory, while on a strictly spatial interpretation, the upward FAC regions are restricted to those in which B_φ falls with time. In the third to fifth panels we then show the electron density n_e, thermal energy W_e, and field-aligned current density $j_{\|}e$ obtained by numerical integration over the observed electron distributions. Within the detectable energy range of the CAPS-ELS instrument it can be seen that the $j_{\|e}$ values are generally significantly smaller than the ionospheric FAC density of $\sim$275 nA m^{-2} estimated in the previous section, indicated within the current region by the red dashed line, such that downward electron acceleration is indeed required. The minimum accelerating voltage $\Phi_\|$ required to produce a FAC density of 275 nA m^{-2} at the ionosphere is shown in the sixth panel (obtained from equation (3a)). As in the CBO models, the accelerating voltages are small, $\sim$0.1–1 kV, where the source plasma is cool dense magnetosheath in character, increasing to $\sim$1–10 kV where the source plasma is warm and tenuous. The seventh panel shows both the in situ electron energy flux E_{fe} (black dots), and the postacceleration value at the ionosphere E_{fI} (equation (3b)) (red dots). The right-hand scale on this panel shows an estimate of the corresponding auroral output on the basis that 1 mW m^{-2} produces $\sim$10 kR of UV emission, while the horizontal dashed line indicates the $\sim$1 kR level of detectability in HST images. It can be seen that precipitation of any of the unaccelerated populations will generally produce emission near or below the limit of detectability. The electron acceleration required to produce $\sim$275 nA m^{-2} at the ionosphere, however, raises the output to $\sim$1–5 kR for the cool dense source plasma, and to $\sim$10–50 kR for the warm tenuous source plasma. While the former values are again near the limit of detectability, the latter correspond reasonably to the typical $\sim$20–30 kR values observed in related HST images. We thus conclude, in line with the results of previous theoretical discussion and modeling [*Cowley et al.*, 2004a, 2004b], that the latter emissions correspond to the principal component of Saturn's main oval auroras.

5. Summary

[20] We present the first simultaneous imaging of Saturn's southern UV aurora by the HST, and in situ observations of Saturn's southern high-latitude magnetosphere by Cassini. The HST images show that the magnetically mapped footprint of the spacecraft during Rev 37 passed directly across the auroral oval near to noon. During this orbit the magnetosphere underwent a shock-compression, such that it should be noted that the observations may well reflect the result of those dynamics, although the precise details of the timing of these effects are unclear. The Cassini plasma electron data show that the oval lies in the boundary between open and closed-field lines, in the cusp region where magnetosheath plasma has access to the magnetosphere. The Cassini magnetic field data show that a major layer of upward-directed FAC lies in the boundary region, indicative of a major shear in the azimuthal magnetospheric flow from strongly sub-corotating flow on open field lines at high latitudes, to near-rigidly corotating flow on closed-field lines at lower latitudes. The implied upward FAC has a density $\sim$275 nA m^{-2} in a layer $\sim$2°–4° colatitude wide in

the ionosphere, integrating to a total current of ~5 MA per radian of azimuth. These observations provide the first in situ evidence of large-scale FACs flowing at the open-closed-field line boundary at Saturn. Comparison of in situ electron fluxes with estimates of the ionospheric FAC density also show that field-aligned acceleration of magnetospheric electrons is required within the current layer, with resulting precipitating energy fluxes that are sufficient to produce UV auroras of several tens kR intensity where the source plasma is warm and tenuous. These emissions then correspond to the observed aurora near to noon. The auroral emissions typically form a quasi-continuous oval, and as such the entire oval is likely also to be associated with the open-closed-field line boundary (although lower latitude emissions may not be). Overall, these results therefore show that the main oval auroras at Saturn are connected with the solar wind interaction like that at Earth, as opposed to being driven by an internal planetary rotation interaction like that at Jupiter, though the currents in the boundary at Saturn are likely determined by flow shears related to rotational dynamics more than to solar wind-driven flows.

[21] **Acknowledgments.** The work presented here relies upon observations made by the NASA/ESA Hubble Space Telescope and the NASA/ESA Cassini-Huygens spacecraft. E.J.B. was supported by PPARC PDF PPA/P/S/2002/00168 and STFC grant PP/E001130/1. CSA was supported by the PPARC/STFC RG to MSSL/UCL. SWHC was supported by STFC grant PPA/E000983/1 and a Royal Society Leverhulme Trust Senior Research Fellowship. Work at Boston was supported by NASA grant HST-GO-10862.01-A from the Space Telescope Science Institute to Boston University. J.C.G. and D.G. are supported by the Belgian Fund for Scientific Research (FNR_S) and by the PRODEX Program managed by ESA in collaboration with the Belgian Federal Science Policy Office. M.K.D. was supported by STFC Senior Fellowship PPA/Y/S/2003/00244. D.L.T. was supported through STFC SG PP/D002117/1.

[22] Wolfgang Baumjohann thanks Donald Mitchell and two other reviewers for their assistance in evaluating this paper.

References

Arridge, C. S., N. Achilleos, M. K. Dougherty, K. K. Khurana, and C. T. Russell (2006), Modeling the size and shape of Saturn's magnetopause with variable dynamic pressure, *J. Geophys. Res.*, *111*, A11227, doi:10.1029/2005JA011574.

Badman, S. V., E. J. Bunce, S. W. H. Cowley, D. Grodent, J.-C. Gérard, and S. E. Milan (2005), Open flux estimates in Saturn's magnetosphere during the January 2004 Cassini-HST campaign, and implications for reconnection rates, *J. Geophys. Res.*, *110*, A11216, doi:10.1029/2005JA011240.

Badman, S. V., S. W. H. Cowley, J.-C. Gérard, and D. Grodent (2006), A statistical analysis of the location and width of Saturn's southern auroras, *Ann. Geophys.*, *24*, 3533–3545.

Bunce, E. J., S. W. H. Cowley, I. I. Alexeev, C. S. Arridge, M. K. Dougherty, J. D. Nichols, and C. T. Russell (2007), Cassini observations of the variation of Saturn's ring current parameters with system size, *J. Geophys. Res.*, *112*, A10202, doi:10.1029/2007JA012275.

Bunce, E. J., C. S. Arridge, S. W. H. Cowley, and M. K. Dougherty (2008), Magnetic field structure of Saturn's dayside magnetosphere and its mapping to the ionosphere: Results from ring current modeling, *J. Geophys. Res.*, *113*, A02207, doi:10.1029/2007JA012538.

Clarke, J. T., D. Grodent, S. W. H. Cowley, E. J. Bunce, P. Zarka, J. E. P. Connerney, and T. Satoh (2004), Jupiter's aurora, in *Jupiter: The Planet, Satellites and Magnetosphere*, edited by F. Bagenal, T. Dowling, and W. McKinnon, Cambridge Planetary Science, Cambridge.

Clarke, J. T., et al. (2005), Morphological differences between Saturn's ultraviolet aurorae and those of Earth and Jupiter, *Nature*, *433*, 717–719.

Connerney, J. E. P., M. H. Acuña, and N. Ness (1983), Currents in Saturn's magnetosphere, *J. Geophys. Res.*, *88*, 8779–8789.

Cowley, S. W. H., and E. J. Bunce (2001), Origin of the main auroral oval in Jupiter's coupled magnetosphere-ionosphere system, *Planet. Space Sci.*, *49*, 1067–1088.

Cowley, S. W. H., and E. J. Bunce (2003), Corotation-driven magnetosphere-ionosphere coupling currents in Saturn's magnetosphere and their relation to the auroras, *Ann. Geophys.*, *21*, 1691–1707.

Cowley, S. W. H., E. J. Bunce, and R. Prangé (2004a), Saturn's polar ionospheric flows and their relation to the main auroral oval, *Ann. Geophys.*, *22*, 1379.

Cowley, S. W. H., E. J. Bunce, and J. M. O'Rourke (2004b), A simple quantitative model of plasma flows and currents in Saturn's polar ionosphere, *J. Geophys. Res.*, *109*, A05212, doi:10.1029/2003JA010375.

Cowley, S. W. H., S. V. Badman, E. J. Bunce, J. T. Clarke, J.-C. Gérard, D. Grodent, C. M. Jackman, S. E. Milan, and T. K. Yeoman (2005), Reconnection in a rotation-dominated magnetosphere and its relation to Saturn's auroral dynamics, *J. Geophys. Res.*, *110*, A02201, doi:10.1029/2004JA010796.

Davis, L., Jr., and E. J. Smith (1990), A model of Saturn's magnetic field based on all available data, *J. Geophys. Res.*, *95*, 15,257–15,267.

Dougherty, M. K., et al. (2005), Cassini magnetometer observations during Saturn orbit insertion, *Science*, *307*, 1266–1270.

Gérard, J.-C., D. Grodent, J. Gustin, A. Saglam, J. T. Clarke, and J. T. Trauger (2004), Characteristics of Saturn's FUV aurora observed with the Space Telescope Imaging Spectrograph, *J. Geophys. Res.*, *109*, A09207, doi:10.1029/2004JA010513.

Grodent, D., J.-C. Gérard, S. W. H. Cowley, E. J. Bunce, and J. T. Clarke (2005), The global morphology of Saturn's southern ultraviolet aurora, *J. Geophys. Res.*, *110*, A07215, doi:10.1029/2004JA010983.

Hill, T. W. (2001), The Jovian auroral oval, *J. Geophys. Res.*, *106*, 8101–8107.

Knight, S. (1973), Parallel electric fields, *Planet. Space Sci.*, *21*, 741–750.

Kurth, W. S., et al. (2005), An Earth-like correspondence between Saturn's auroral features and radio emission, *Nature*, *433*, 722–725.

Sittler, E. C., Jr., M. F. Blanc, and J. D. Richardson (2006), Proposed model for Saturn's auroral response to the solar wind: Centrifugal instability model, *J. Geophys. Res.*, *111*, A06208, doi:10.1029/2005JA011191.

Southwood, D. J., and M. G. Kivelson (2001), A new perspective concerning the influence of the solar wind on Jupiter, *J. Geophys. Res.*, *106*, 6123–6130.

Zieger, B., and K. C. Hansen (2008), Statistical validation of a solar wind propagation model from 1 to 10 AU, *J. Geophys. Res.*, *113*, A08107, doi:10.1029/2008JA013046.

C. S. Arridge and A. J. Coates, Mullard Space Science Laboratory, University College London, Dorking RH5 6NT, UK.

E. J. Bunce, S. W. H. Cowley, and D. L. Talboys, Department of Physics and Astronomy, University of Leicester, University Road, Leicester LE1 7RH, UK. (emma.bunce@ion.le.ac.uk)

J. T. Clarke and J. D. Nichols, Center for Space Physics, Boston University, 725 Commonwealth Avenue, Boston, MA 02215, USA.

M. K. Dougherty, Blackett Laboratory, Imperial College, London SW7 2BZ, UK.

J.-C. Gérard and D. Grodent, Laboratoire de Physique Atmosphérique et Planétaire, Université de Liège, B-4000 Liège, Belgium.

K. C. Hansen, Department of Atmospheric, Oceanic, and Space Sciences, University of Michigan, Ann Arbor, MI 48109, USA.

D. J. Southwood, European Space Agency, HQ, 75738 Paris, France.